New Red Phosphor Ceramic $K_2SiF_6:Mn^{4+}$

R.A. Osborne[a], N.J. Cherepy[a], Z.M. Seeley[a], S.A. Payne[a], A. D. Drobshoff[a], A.M. Srivastava[b], , W.W. Beers[b], W.W. Cohen[b], D. L. Schlagel[c]

[a] Lawrence Livermore National Laboratory, Livermore, CA, 94550, United States

[b] GE Current, a Daintree company, 1099 Ivanhoe Road, Cleveland, Ohio 44110

[c] Ames Laboratory, Ames, IA, 50011 Unites States

[*] Corresponding author, N. Cherepy, Email address: cherepy1@llnl.gov

ABSTRACT:

A new transparent ceramic phosphor for use in LED lighting has been fabricated. The previously reported and optimized narrow-emitting red phosphor, $K_2SiF_6:Mn^{4+}$ (KSF), has been consolidated into a transparent ceramic phosphor for the first time, accomplished via hot-pressing the feedstock phosphor powder in a die under vacuum. KSF ceramics were synthesized with varying doping concentrations of Mn^{4+} and their properties studied. The absorption and emission spectra of the ceramics were identical to the feedstock phosphor powders and are ideal for LED lighting with strong absorption at 450 nm and narrow emission around 630 nm. The absorbance of the ceramics was directly proportional to the doping concentration. The ceramics were excited at various light fluxes and their emission intensities measured to study the effect of Mn^{4+} concentration on intensity-driven "droop" in the emission output. The ceramics with a lower Mn^{4+} doping were more efficient under higher light fluxes due to a decrease in Auger upconversion losses. KSF ceramics can allow a much longer path length of the diode light through the phosphor, as compared to phosphor-in-silicone, enabling the use of low optical absorption and the associated reduced activator concentration. The ceramics are measured to have a thermal conductivity of ~1.0 W/m-K, higher than that of phosphor-in-silicone or phosphor-in-glass. Several of these properties make KSF ceramics potentially desirable for use in white light LEDs. Greater thermal conductivity helps with heat dissapation, the lower surface area of the ceramic compared to the powder minimizes the environmental vulnerability of KSF, and the ability to lower the Mn^{4+} concentration reduces Auger recombination losses and the temperature rise, particularly at higher light flux.

Keywords

Phosphor ceramic
Transparent ceramic
Red phosphor
K_2SiF_6
LED phosphor
Droop

Abbreviations: $K_2SiF_6:Mn^{4+}$ (KSF), $Y_3Al_5O_{12}:Ce^{3+}$ (YAG:Ce)

1. Introduction

Commercial, residential and specialty lighting are rapidly shifting toward phosphor converted white Light Emitting Diodes (pc-LEDs). The ongoing replacement of other lighting technologies by LEDs is driven by their greater efficiency, longer lifetime, color quality, decreasing cost, decreased rare earth element usage (compared to fluorescent lighting), and lack of toxic materials [1-3]. In pc-LEDs, a blue-emitting InGaN chip is coupled to one or more phosphors, typically one or more green-yellow Cerium-doped garnet phosphors, along with a red phosphor that is often added to induce a "warm-white" color temperature (1800-3000 K). Red phosphors for LED lighting have been the subject of much recent research, requiring both strong absorption at 450 nm and narrow emission around 630 nm with minimal emission beyond 650 nm for optimal efficiency [2, 4]. $K_2SiF_6:Mn^{4+}$ (KSF) is a red phosphor that has an ideal emission spectrum, due to its sharp peaks around 630 nm. Much research has been conducted to optimize the efficiency, environmental stability, and synthesis of KSF [5-8]. KSF has already been commercially implemented in LED lighting fixtures and shown to improve efficiency by >10%, compared to fixtures with conventional Eu^{2+}-doped nitride phosphors which have broad emission spectra [9].

LED packages typically utilize a phosphor-in-silicone matrix to coat the LED chip, which works well for low to moderate blue-light flux. However, for high drive applications, e.g. in automobile headlights, monolithic translucent ceramic phosphors are often used. Some phosphor ceramics that have been reported are yellow-emitting YAG:Ce [10] and red-emitting $CaAlSiN_3$:Eu [11, 12]. Phosphor ceramics offer several advantages over phosphor-in-silicone, including greater thermal conductivity and improved environmental stability. The thermal conductivity at room temperature of phosphor-in-silicone ranges from 0.1-0.4 W/m-K (depending on the type of silicone, phosphor, and the phosphor loading) [13], while phosphor-in-glass (PiG) has been reported at 0.71 W/m-K [14], single crystal YAG offers 14 W/m-K, ceramic YAG:Ce ranges between 6-10 W/m-K, mixed YAG:Ce / Al_2O_3 composites reach 18.5 W/m-K [15], and $CaAlSiN_3$:Eu ceramics provide 4 W/m-K [11]. Higher thermal conductivity helps with heat dissipation, as thermal quenching can reduce quantum efficiency at elevated temperatures. This is especially important in high light flux applications.

Phosphor ceramics also enable greater design flexibility for phosphor layer thickness, activator concentration, and control of optical scatter which is also advantageous for high light flux applications. Transparent or translucent phosphor ceramics may be designed for a much longer pump light path length, compared to highly-scattering phosphor powder compacts. This longer path length allows for lower activator concentrations, reducing losses from concentration quenching, dynamic excited-state effects, and thermal quenching, thereby improving the high temperature and high light flux efficiency [13]. Droop in phosphors is a phenomenon describing their tendency to lose efficiency as the light flux increases due to excited-state upconversion losses. This is of great concern for phosphors used in solid-state lighting because not only does it result in a loss of luminous efficiency, but also a pump-dependent color shift in a mixed-phosphor lamp where the phosphors exhibit differential droop [16]. Droop has been reported in the commonly used LED phosphors $Y_3Al_5O_{12}:Ce^{3+}$, $CaAlSiN_3:Eu^{2+}$, and $(Ba,Sr)_2Si_5N_8:Eu^{2+}$ [17-

19]. Reduced thermal quenching and droop may be achieve by reducing the activator concentration, as has been reported in $Y_3Al_5O_{12}:Ce^{3+}$ and $(Ba,Sr)_2Si_5N_8:Eu^{2+}$, respectively [16, 20].

Phosphor ceramics offer greater durability compared to phosphor-in-silicone, which can degrade over time due to significant heating from the diode [21]. Dense polycrystalline ceramics have significantly reduced phosphor surface area, compared to standard powder phosphors with ~10 micron grains. This reduces adsorption of oxygen and moisture which react with some phosphors. In the case of KSF, moisture is known to degrade the efficiency through hydrolysis of Mn to produce dark colored Mn oxides and hydroxides, although surface treatments have mitigated this issue [6, 9].

In this work, the red phosphor, KSF, was fabricated for the first time into a transparent, polycrystalline ceramic. The excitation and absorption of the ceramics were characterized as a function of Mn^{4+} concentration, as well as the droop behavior.

2. Experimental Procedure

2.1. Powder Synthesis

$K_2SiF_6:Mn^{4+}$ phosphor powders of Mn-doping concentrations ranging from 0 wt% to 2.5 wt% of Mn on the Si site, equivalent to x = 0 – 0.013 in the formula $K_2(Si_{1-x}Mn_x)F_6$, were synthesized by GE Current. Mn concentrations reported in this work are in weight percent on the Si site. All powders were stored in an argon-filled glovebox prior to use.

Undoped K_2SiF_6 (Sigma-Aldrich, 99%) was purified by treatment under flowing HF gas at 400°C for 15 minutes in a platinum boat.

2.2. Ceramic Synthesis

The KSF powders were loaded into a 12.7 mm diameter steel die lined with graphite foil in an argon-filled glovebox. The die was then loaded into a uniaxial hot-press and pressed under vacuum ($\leq 3.0 \times 10^{-3}$ mTorr) at approximately 25,000 psi and ~500°C and held for one hour. The temperature ramp rate was 10°C/min (upward and downward) and pressure was not applied until the dwell temperature was reached. Pressure was slowly released at the end of the dwell. The surfaces of the ceramics were polished with a solution of sodium lauryl sulfate and 0.5 µm diamond grit on a soft pad.

2.3 Physical Characterization

Thermal conductivity measurements of a 1 wt% Mn-doped KSF ceramic were performed by Netzsch Instruments North America, LLC. Thermal diffusivity and specific heat were measured at 25 and 200 ºC by the flash method using a NETZSCH LFA 467 HyperFlash™ instrument. This instrument and the test method conform to ASTM E1461-13, “Standard Test Method for Thermal Diffusivity by the Flash Method”. Prior to testing, the sample was coated with approximately 5 µm of graphite.

X-ray diffraction was performed on the ceramic samples with a Bruker AXS D8 ADVANCE X-ray diffractometer with a Cu anode ($K_{\alpha 1}$ = 0.1540598 nm).

Examination of particle morphology was performed using a Phenom ProX desktop scanning electron microscope. Micrographs were collected in backscattered electron mode using an accelerating voltage of 15 kV, working distance of 11.5 mm, and a spot size of 5.5 mm. Samples were prepared by dispersing the powder onto conductive carbon tape.

2.4. Luminescence Spectroscopy

To measure the luminescence characteristics of the as-synthesized powders, they were mixed into a fluoropolymer dissolved in acetone. The acetone was then evaporated to leave behind a film of the phosphor in the fluoropolymer. Ceramics were measured in backscatter geometry with Teflon backing to allow for a "double pass" of the excitation in high transparency samples. Emission and excitation spectra were measured with a Thermo Lumina luminescence spectrometer using backscatter geometry, excitation and emission slits of 1 nm, a signal averaging time of 0.2 s per point, and a scan rate of 300 nm/minute. To estimate the quantum efficiencies of compounds, their integral light yields were compared to that of commercial Intematix Cerium-doped Yttrium Aluminum Garnet powder, product NYAG-4156, which offers quantum efficiency of approximately unity.

2.5. Thermal Dependence of Luminescence

To measure the effect of temperature on the efficiency of the KSF powders, the powder was compacted onto a heating stage and a glass slide placed over it. The ceramics were similarly placed onto a heating stage with a glass slide placed on top. The samples were then excited at 450nm and their emission intensity measured as the heating stage temperature was increased from room temperature to 300°C. The heating stage temperature was held for each data point until the system reached steady-state, indicated by a constant emission intensity. A low excitation intensity was used so that there would not be appreciable heating from the phosphor itself.

2.6. Droop and Bleaching Measurements

The emission droop and transmission bleaching experiments were performed utilizing a fiber-coupled 450 nm pulsed laser diode (Oxxius model LBX-450-1200-HPE-PP). The measured wavelength was 447.3nm. A 50 mm focal length lens was used to image the 200 μm fiber to a 400 μm spot size on the KSF sample. Three amplified silicon photodiodes were employed to detect the emission, transmitted light, and a reference to the diode output. Both 495 nm and 515 nm long pass filters were used on the photodiode measuring the fluorescence. The pulse shapes were stored on a Keysight 3034T digital oscilloscope.

3. Results and Discussion

3.1 Physical Characteristics

The KSF powders from GE had a light-yellow body color and deepened in color as a function of increasing Mn concentration, due to an increased absorption coefficient. The particle morphology can be seen in the SEM image in Figure 1. The particles were highly crystalline and primarily cuboidal with some faceted corners and formed loose agglomerates of several crystallites. The average particle size was ~25 µm.

The produced samples were approximately 12.5 mm in diameter and 2 mm in thickness. Samples from 0.04 – 1 wt% Mn are shown in Figure 2. It was confirmed via x-ray diffraction that the samples were pure phase cubic K_2SiF_6. The body-color was yellow-orange and deepened as the manganese concentration increased. The luminescence was deep red under UV to 450nm excitation and the same color for all dopant concentrations. The samples were transparent, as can be seen in Figure 2. The samples had relatively low scatter for the intended application of implementation in an LED package. However, it could be advantageous to introduce more scatter to diffuse the light and increase the path length so that the diode light has more chance of being absorbed by the phosphor for the case of using transparent ceramics in an actual lamp [15]. This could be achieved by introducing "defects" such as pores or reflective secondary phase particles.

The undoped KSF (Sigma-Aldrich, 99%) was white and crystalline. This material was hot-pressed as-received, as well as after the HF treatment described above. The as-received KSF produced an opaque, off-white sample; however, the HF treated KSF produced a transparent, colorless sample. It was hypothesized that moisture on the surface of the particles may react with a fraction of the particles creating a small fraction of an oxyfluoride or oxide, causing the hot-pressed ceramic to be opaque, but the HF treatment removes water from the surface of the particles, allowing a pure-phase transparent ceramic to be formed from the powder.

The ceramics were brittle and prone to cracking in the pressing step. This problem was resolved by lining the inside of the steel die with graphite foil. It likely that the graphite foil prevents the KSF from sticking to the inside of the die and causing cracking during cooling from stress due to the thermal expansion difference between KSF and steel, or reduces friction between the KSF and the inside of the die while pressing the sample out which could put strain on the sample (also causing it to crack). The specific heat, thermal diffusivity, and thermal conductivity were measured at 25°C and 200°C for a 1 wt% Mn-doped KSF ceramic; the values are shown in Table 1. The measured thermal conductivity of approximately 1.0 W/m-K in the range of 25 – 200°C is greater than the reported 0.1 – 0.4 W/m-K for phosphor-in-silicone [13] and 0.71 W/m-K for PiG, but significantly less than ceramic YAG:Ce (6-10 W/m-K) and $CaAlSiN_3$:Eu (4 W/m-K) [11]. Implementing KSF in a ceramic form, rather than phosphor-in-silicone or PiG, therefore has the potential to improve heat dissipation from the phosphor. Also, the thermal conductivity of KSF ceramics could potentially be improved by reducing defects through improved synthesis conditions or altering the Mn-concentration.

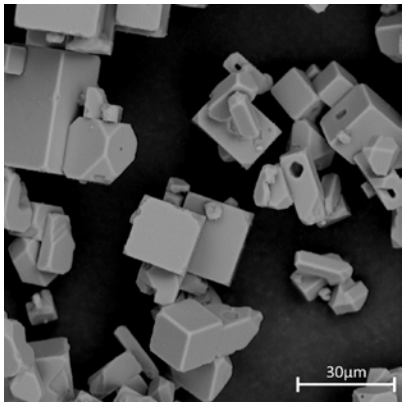

Figure 1. SEM image of KSF powder revealing the typically cuboidal shape and primary particle size of 5-50 µm.

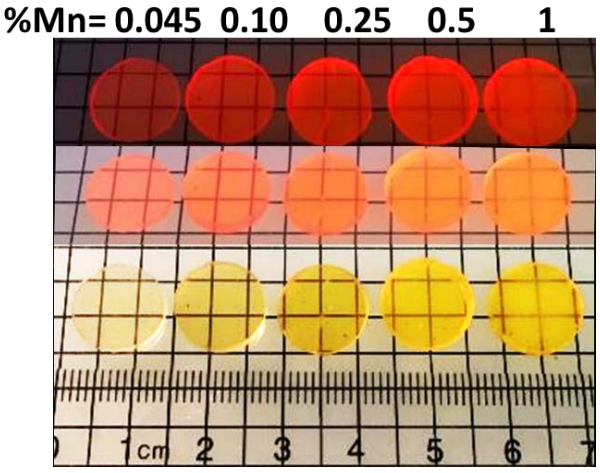

Figure 2. KSF ceramics of doping levels ranging from 0.045 – 1 wt% Mn. **(top)** Under 254 nm excitation in darkness, **(middle)** Under 365 nm excitation in room lights, **(bottom)** In room lights. None of the photos are backlit.

Table 1. Flash method thermal conductivity results of a 1 wt% Mn-doped KSF ceramic.

ASTM E1461 Flash Method Thermal Conductivity Results

Sample	thickness Δx (mm)	bulk density ρ (g/cm^3)	temperature T (°C)	specific heat c_p (J/g-K)	diffusivity α (mm^2/s)	conductivity λ (W/m-K)
RAO-I-120H	1.95	2.33	25	0.963	0.431	0.967
			200	1.52	0.294	1.05

3.2 Luminescence

The absorption and emission spectra of the KSF ceramics is identical to the powders from which they were pressed, indicating that the local electronic structure of the Mn^{4+} ions was not effected by the consolidation of the powder into a ceramic. They have two absorption bands between approximetly 320 – 380 nm and 400 – 500 nm, shown in Figure 3, and arising from the indicated transitions. The Mn content of the ceramics does not affect the shape or position of the absorption bands in this range, only the intensity of absorption is affected. The absorption coefficient increases linearly with Mn concentration, as seen in the inset in Figure 3, where the absorbance is defined as the optical density divided by the sample length.

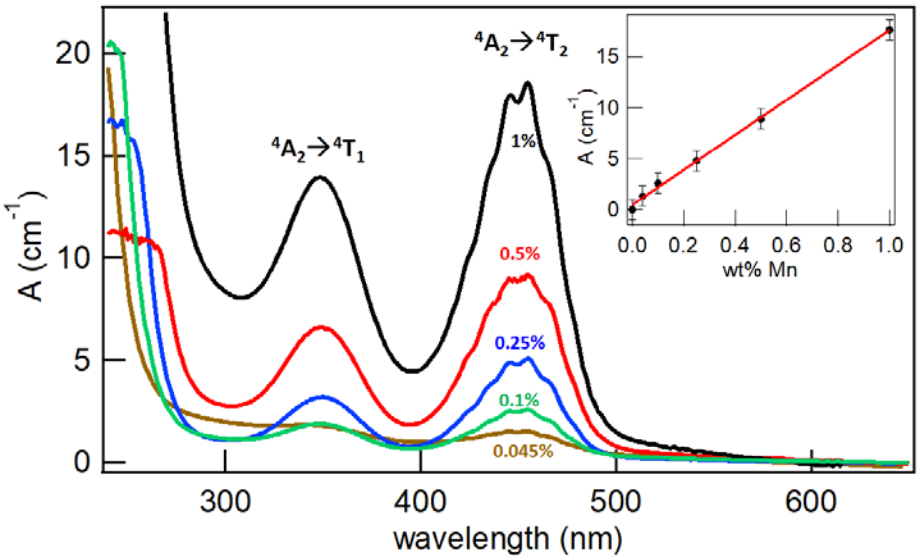

Figure 3. Absorbance of KSF ceramics with 0.045 – 1 wt% Mn. **Inset**: Absorbance at 450nm.

The KSF ceramics exhibit red luminescence with five sharp peaks in the 600 – 650nm range as shown in Figure 4, in agreement with the typical reported luminescence of $K_2SiF_6:Mn^{4+}$ [5, 6]. The emission intensity increases with Mn concentration, as shown in the inset in Figure 4. The emission intensity appears to start leveling off at higher concentrations (>0.25 wt%) of Mn, due to nearly complete absorption of the excitation light at high Mn concentrations. This is qualitatively in agreement with measurements of the diffuse reflectance spectra, shown in Figure 5, and the measured emission intensity, shown in Figure 6, of thin films of KSF powders suspended in a fluoropolymer. The diffuse reflectance decreases with increasing Mn concentration, with diffuse reflectance of undoped KSF taken as 100% at 450nm to approximately 35% at 2.5 wt% Mn-doped KSF. The emission intensity and absorbance of the films are plotted in Figure 6. Both increase proportionally up to 1.5 wt% Mn, indicating that the quantum efficiency is staying consistently high. Above 1.5 wt% Mn however, concentration quenching appears to set in as the absorption continues to increase, but the emission intensity does not.

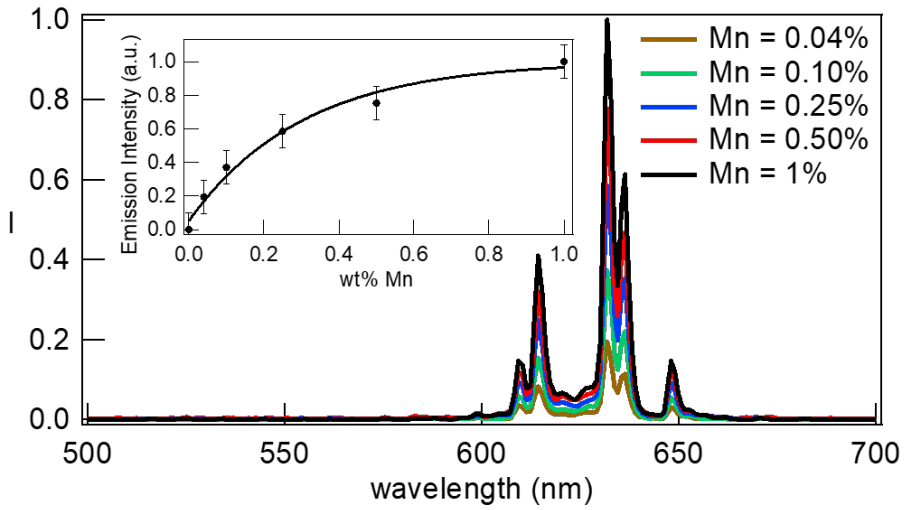

Figure 4. Emission spectra acquired with 450 nm excitation of the KSF ceramics shown in Figure 2. **Inset:** Emission intensity is relative to the 1 wt% Mn-doped sample.

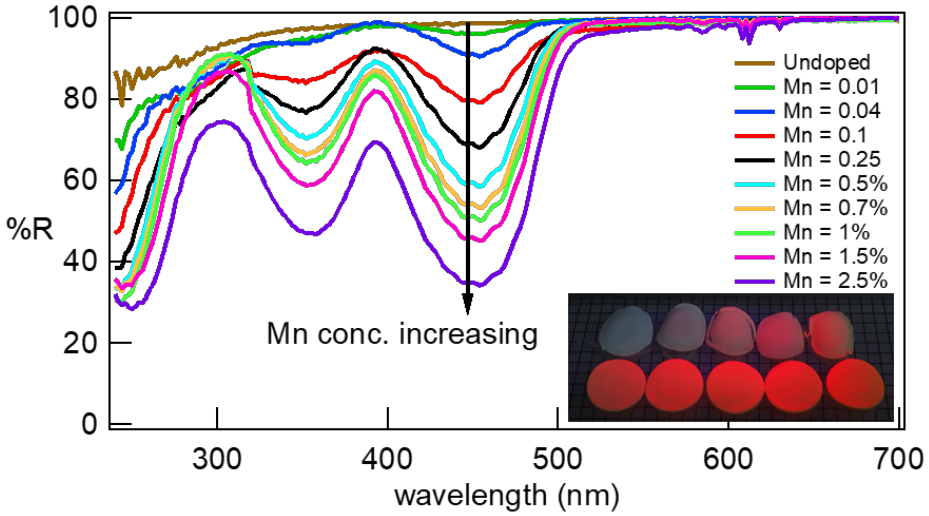

Figure 5. Diffuse reflectance spectra acquired of KSF films of various doping levels. **Inset:** Films used for measurements, under UV excitation.

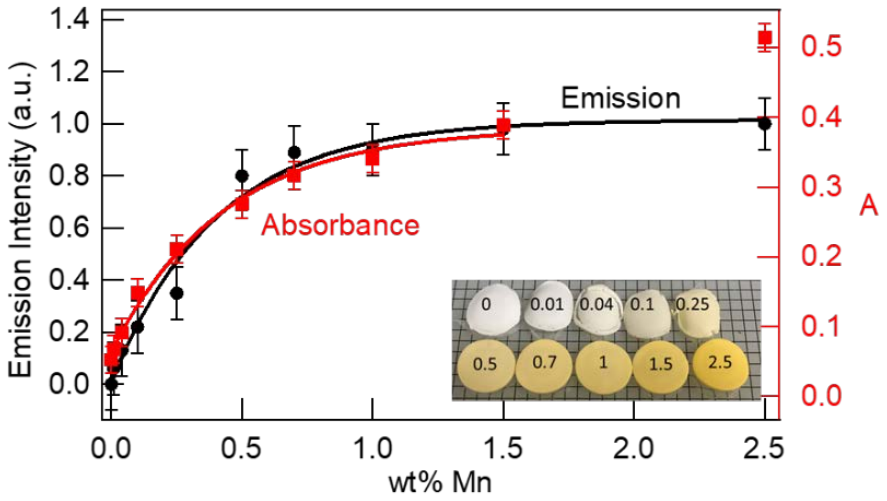

Figure 6. Emission and absorbance of KSF films. **Inset:** Films used for measurements.

The measured thermal dependence of luminescence of 1 wt% Mn-doped powder and ceramic is shown in Figure. 7. The thermal quenching results for the powder agree with the previously reported thermal quenching behavior for KSF [22]. The ceramic is observed to thermally quench much less than the powder at higher temperatures. However, the temperature was measured at the heating stage (not on the sample directly), and the sample was irradiated from the top, through the glass slide so most absorption and emission would occur near this surface. Therefore, it is likely that the higher thermal conductivity of the ceramic allowed for greater heat conduction into the glass slide placed on top of it, making this surface cooler than the heating stage. To account for this effect, we deduced the actual ceramic temperature using the ratio of the Stokes and anti-Stokes peaks at 633 nm and 615 nm, respectively, see Figure 8. The ceramic and powder have a ratio of ~2.5 at room temperature which decreases at higher heating stage temperature. Since the slope is shallower for the ceramic than the powder, this indicates that the ceramic's temperature at the irradiated surface is less than that of the heating stage. Using the data in Figure 8, we can deduce the actual sample temperature for the ceramic, as plotted in Figure 9; this result indicates that the thermal quenching behavior for the ceramic is essentially the same as for the powder, as one might expect to be the case.

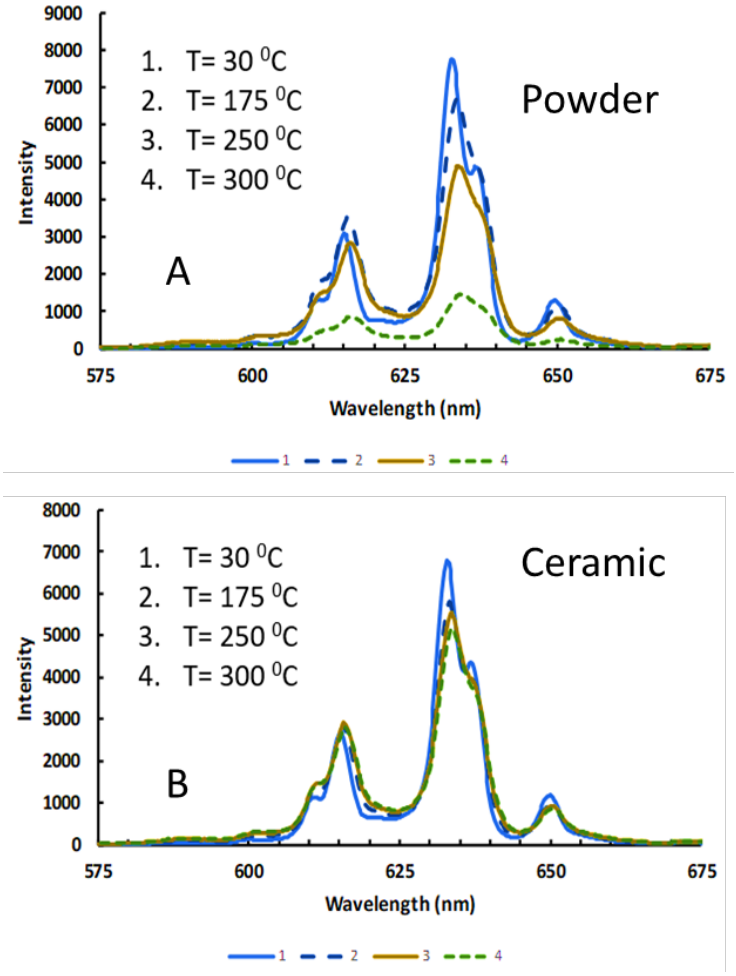

Figure 7. (a) Thermal quenching results for 1 wt% Mn-doped KSF powder (b) and ceramic.

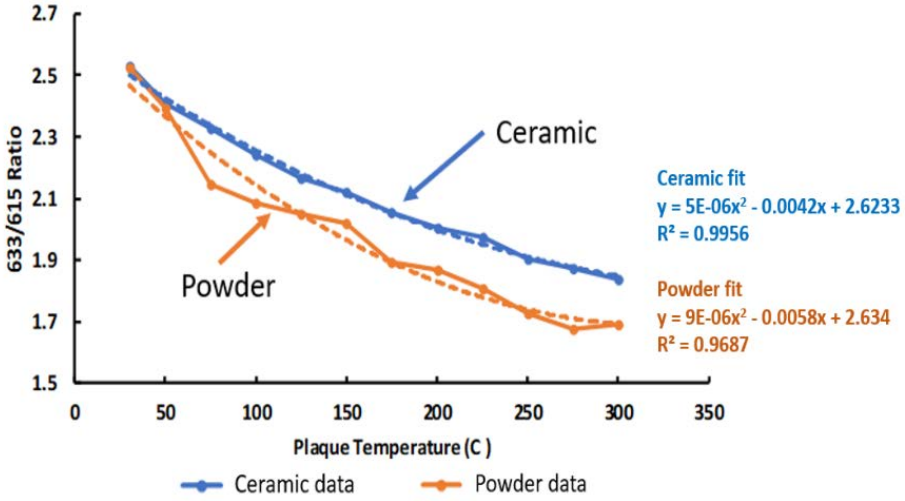

Figure 8. Stokes to anti-Stokes ratio of peak intensity as a function of heating stage temperature for KSF ceramic and powder from data in Figure. 7.

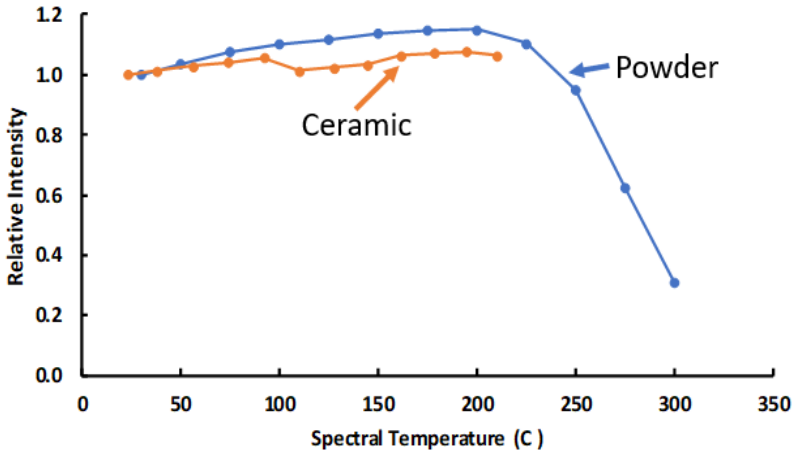

Figure 9. Relative intensity as a function of the actual sample temperature deduced by the Stokes/anti-Stokes peak intensity ratio.

3.3 Droop Results

To study the emission behavior of KSF ceramics at different Mn concentrations, ceramics of similar thickness and various Mn concentrations were excited with a blue laser with a defined intensity and their relative emission measured under the same experimental conditions for all samples. The experimental results were then modeled on the basis of two numerically iterated equations, Equations 1 and 2, for the pump intensity as it traversed the sample and the excited-state density as a function of time, yielding intensity and excited state density as a function of both time and position.

Eq. 1 $$\frac{I(x+\Delta x,t)}{I(x,t)} = 1 - \{\sigma_{abs}[N_0 - N_{ex}(x,t)] + \sigma_{ESA}N_{ex}(x,t)\}\Delta x$$

Eq. 2 $$N_{ex}(x,t+\Delta t) - N_{ex}(x,t) =$$

$$\{\sigma_{abs}[N_0 - N_{ex}(x,t)]\frac{I(x,t)}{h\nu} - [\alpha_{ESA}\sigma_{ESA}N_{ex}(x,t)]\frac{I(x,t)}{h\nu} - \gamma_A N_{ex}(x,t)^2 - \frac{N_{ex}(x,t)}{\tau_{em}}\}\Delta t$$

Here, I = pump light intensity (W/cm^2), σ_{abs} = ground-state absorption cross section (cm^2), σ_{ESA} = excited-state absorption cross section (cm^2), N_0 = Mn doping density (cm^{-3}), N_{ex} = Mn excited state density (cm^{-3}), hν = pump photon energy (J), γ_A = Auger upconversion coefficient (cm^{3}s^{-1}), α_{ESA} = fraction of events leading to a "lost" excited-state, and τ_{em} = emission lifetime (ms).

In order to iterate these equations, the step sizes Δx and Δt, must be small compared to the sample length and the emission lifetime (τ_{em}), respectively. The equations were solved to model the experimental results as follows:

1. Calculate I(x, 0) for all N_{ex}(x, 0) = 0 from 0 < x < ℓ using Eq. 1
2. Insert I(x, 0) into Eq. 2 to calculate N_{ex}(x, Δt)
3. Insert N_{ex}(x, Δt) into Eq. 1 to calculate I(x, Δt)

4. In succession, continue to use I(x, Δt) to calculate $N_{ex}(x, 2\Delta t) \rightarrow I(x, 2\Delta t)$ and so on
5. At the termination of the blue pump pulse time, set I = 0 and allow the evolution of Eq. 2 to henceforth be followed

Figure 9 shows the experimental data and model prediction of relative emission intensity and bleaching for three KSF ceramics of different Mn concentrations. The values used to model the experimental data employing Equations 1 and 2 are in Table 2. Auger upconversion is identified as a mode of non-radiative excited-state losses in KSF. Auger upconversion occurs when one excited Mn ion is promoted to a higher energy electronic state using energy from a second excited Mn ion that then transitions to its ground state (conserving the overall energy). Notice in Table 2 that the Auger upconversion coefficient increases with increasing Mn concentration. The observed concentration dependence of Auger upconversion is due to enhanced energy migration among the Mn ions, which allows the excited states to come into closer proximity.

The fraction of excitation light transmission must be measured, as well, because "bleaching" can occur at high light flux, when a significant fraction of ground-state Mn^{4+} ions are excited. As a result, the relative transmission of excitation light through the sample increases with bleaching because the sample essentially becomes less absorptive. Substantial bleaching occurs even at low light fluxes for samples with low activator concentrations, because there are fewer Mn^{4+} ions to excite. The highest doped sample exhibits the largest change in transmission with increasing excitation flux, due to the increased level of bleaching (see Figure 9). Both the emission intensity and emission droop were measured and fit to a common set of spectroscopic parameters, which proved to be a stringent test of the model's validity.

The predicted droop for three KSF ceramics at different concentrations of Mn with constant optical absorption, where longer sample lengths correspond to lower doping, are shown in Figure 10 using the parameters in Table 2. The 0.045% Mn-doped sample is calculated to be 85% as efficient at 300 W/cm^2 as it is at a very low light flux, whereas the 0.25% Mn-doped sample exhibits more droop and is only 72% as efficient at 300 W/cm^2.

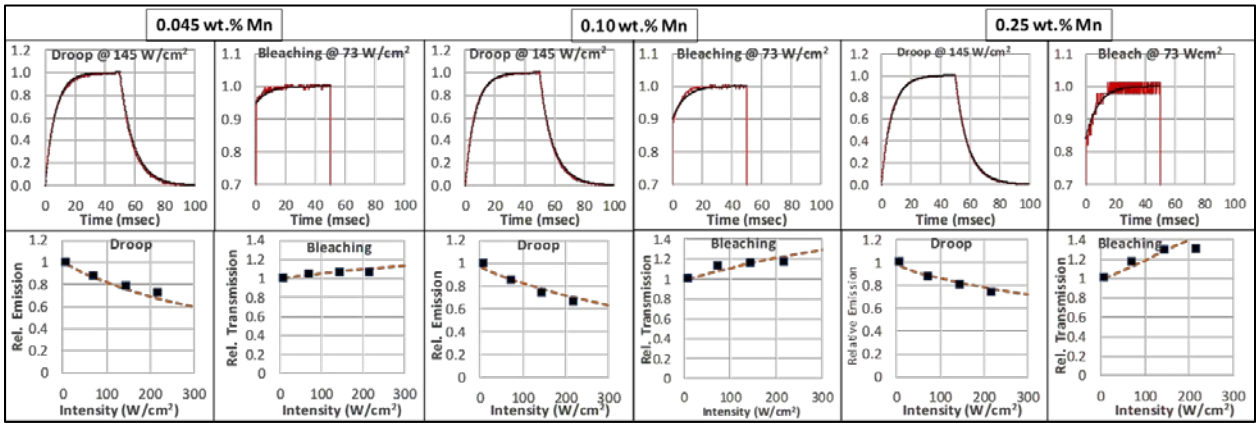

Figure 9. Examples of the relative emission intensity and bleaching dependence for KSF ceramics with three Mn concentrations and at selected excitation intensities. The temporal measurements are plotted in the upper part of the Figure (red lines are data, black are fits), while

the integrated emissions and maximum bleaching levels are plotted as a function of the pump intensity in the lower part of the Figure (square points are data, dotted lines are fits).

Table 2. Values derived from the model of droop and bleaching for each of the three samples.

Fitting parameters for KSF:Mn Ceramics			
Mn doping	0.045%	0.10%	0.25%
Doping level (cm^{-3}), N_0	1.34E+19	2.98E+19	7.45E+19
Emission Lifetime (ms), τ_{em}	9.4	9.4	9.4
Auger upc. coeff. (cm^3s^{-1}), γ_A	4.00E-19	7.00E-19	1.30E-18
GS cross section (cm^2), σ_{abs}	1.5E-19	1.5E-19	1.5E-19
ESA cross section (cm^2), σ_{ESA}	1.5E-20	1.5E-20	1.5E-20
Sample length (cm), ℓ	0.173	0.185	0.236
Beam radius (mm)	0.355	0.355	0.355
ESA lost fraction, α_{ESA}	0.70	0.70	0.70

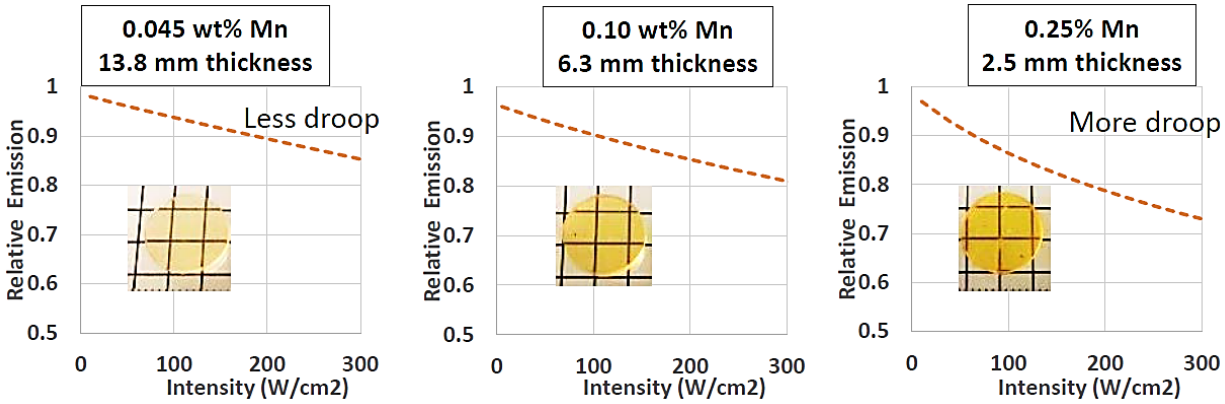

Figure 10. Calculations of droop for three Mn concentrations at constant optical absorption in KSF ceramics.

In pc-LEDs utilizing KSF powder-in-silicone, KSF is used with a relatively high concentration of ≥1 wt% Mn^{4+} (i.e. 4x greater that the highest concentration in Figure 10). This is because a strong absorption coefficient is required for phosphor-in-silicone due to the medium being highly scattering; if too much phosphor powder were added, the silicone layer would become close to opaque. The path length of the diode light is thus very short, requiring strongly absorbing phosphor particles. KSF ceramics, however, could be utilized with much lower dopant concentrations such as 0.05 – 0.25 wt% Mn. Since the ceramics are very low scattering, a much longer path length through the KSF is possible compared to the phosphor-in-silicone, and a high absorption coefficient is not needed. This creates the potential to make pc-LEDs with KSF more efficient, particularly at higher light fluxes due to decreased droop.

4. Conclusion

The narrow-emitting red phosphor, KSF, has been consolidated into a transparent ceramic for the first time through a hot-pressing process, using KSF powders with various Mn^{4+} doping concentrations that were synthesized at General Electric. The thermal conductivity was measured to be superior to that of the phosphor-in-silicone or phosphor-in-glass values. The ceramics were shown to have the same absorption and emission spectra as the feedstock powder as well as being equally efficient. The absorption coefficient and induced emission of the ceramics excited at 450 nm increased as a function of dopant concentration, as expected. The droop behavior of the ceramics was measured and it was found that there was less decrease in efficiency at high intensity light pumping for the samples with lower Mn^{4+} concentrations. This was determined to be due to the lower activator concentration, mitigating Auger upconversion. The KSF ceramics allow a much longer path length of the diode light through the phosphor than is the case for phosphor-in-silicone, enabling the use of lower Mn^{4+} concentrations to take advantage of the improved droop behavior. Several properties render KSF ceramics potentially desirable for use in white light LEDs as an alternative to particles-in-silicone: greater thermal conductivity assists with heat dissapation, lower surface area reduces the environmental vulnerability, and lower Mn^{4+} concentration reduces Auger upconversion losses and the associated temperature rise, particularly at higher light fluxes.

Declaration of Interests

The authors declare no known financial interests or personal relationships which could influence the work or content present in this paper.

Acknowledgments

We acknowledge helpful discussions with Thomas Lagrasso at Ames Laboratory. Funding was provided by the DOE EERE Critical Materials Institute, and work was performed under the auspices of the U.S. Department of Energy by Lawrence Livermore National Laboratory under Contract DE-AC52-07NA27344. The work performed at Ames Laboratory, which is operated for the U.S. DOE by Iowa State University, was under contract DE-AC02-07CH11358. The release number is LLNL-JRNL-810280.

Dr. Srivastava is a consultant to GE Current and he can be reached at srivastaam@outlook.com

References

[1] M. Yamada, K. Stober, Adoption of light-emitting diodes in common lighting applications, Navigant, Chicago, IL (United States), (2015). http://doi.org/10.2172/1374108.

[2] P. Pust, P.J. Schmidt, W. Schnick, A revolution in lighting, Nature materials, 14 (2015) 454-458. https://doi.org/10.1038/nmat4270.

[3] A.Y. Ku, A.A. Setlur, J. Loudis, Impact of light emitting diode adoption on rare earth element use in lighting: Implications for yttrium, europium, and terbium demand, The Electrochemical Society Interface, 24 (2015) 45-49. https://doi.org/10.1149/2.F04154if.

[4] J.L. Leaño, M.-H. Fang, R.-S. Liu, Critical review—narrow-band emission of nitride phosphors for light-emitting diodes: perspectives and opportunities, ECS Journal of Solid State Science and Technology, 7 (2018) R3111-R3133. https://doi.org/10.1149/2.0161801jss.

[5] H.F. Sijbom, R. Verstraete, J.J. Joos, D. Poelman, P.F. Smet, K2SiF6:Mn4+ as a red phosphor for displays and warm-white LEDs: a review of properties and perspectives, Opt. Mater. Express, 7 (2017) 3332-3365. https://doi.org/10.1364/OME.7.003332.

[6] L. Huang, Y. Liu, J. Yu, Y. Zhu, F. Pan, T. Xuan, M.G. Brik, C. Wang, J. Wang, Highly STable K2SiF6:Mn4+@K2SiF6 Composite Phosphor with Narrow Red Emission for White LEDs, ACS Applied Materials & Interfaces, 10 (2018) 18082-18092. https://doi.org/10.1021/acsami.8b03893.

[7] R. Verstraete, H.F. Sijbom, J.J. Joos, K. Korthout, D. Poelman, C. Detavernier, P.F. Smet, Red Mn4+-Doped Fluoride Phosphors: Why Purity Matters, ACS Applied Materials & Interfaces, 10 (2018) 18845-18856. https://doi.org/10.1021/acsami.8b01269.

[8] M.J. Lee, Y.H. Song, Y.L. Song, G.S. Han, H.S. Jung, D.H. Yoon, Enhanced luminous efficiency of deep red emitting K2SiF6:Mn4+ phosphor dependent on KF ratio for warm-white LED, Materials Letters, 141 (2015) 27-30. https://doi.org/10.1016/j.matlet.2014.11.025.

[9] J.E. Murphy, F. Garcia-Santamaria, A.A. Setlur, S. Sista, 62.4: PFS, K2SiF6:Mn4+: the Red-line Emitting LED Phosphor behind GE's TriGain Technology™ Platform, SID Symposium Digest of Technical Papers, 46 (2015) 927-930. https://doi.org/10.1002/sdtp.10406.

[10] S. Nishiura, S. Tanabe, K. Fujioka, Y. Fujimoto, Properties of transparent Ce: YAG ceramic phosphors for white LED, Optical Materials, 33 (2011) 688-691. https://doi.org/10.1016/j.optmat.2010.06.005.

[11] S. Li, Q. Zhu, L. Wang, D. Tang, Y. Cho, X. Liu, N. Hirosaki, T. Nishimura, T. Sekiguchi, Z. Huang, CaAlSiN 3: Eu 2+ translucent ceramic: a promising robust and efficient red color converter for solid state laser displays and lighting, Journal of Materials Chemistry C, 4 (2016) 8197-8205. https://doi.org/10.1039/C6TC02518H.

[12] S. Li, D. Tang, Z. Tian, X. Liu, T. Takeda, N. Hirosaki, F. Xu, Z. Huang, R.-J. Xie, New insights into the microstructure of translucent CaAlSiN3:Eu2+ phosphor ceramics for solid-state laser lighting, Journal of Materials Chemistry C, 5 (2017) 1042-1051. https://doi.org/10.1039/C6TC04987G.

[13] M. Raukas, J. Kelso, Y. Zheng, K. Bergenek, D. Eisert, A. Linkov, F. Jermann, Ceramic phosphors for light conversion in LEDs, ECS Journal of Solid State Science and Technology, 2 (2013) R3168-R3176. http://dx.doi.org/10.1149/2.023302jss.

[14] R. Zhang, H. Lin, Y. Yu, D. Chen, J. Xu, Y. Wang, A new-generation color converter for high-power white LED: transparent Ce3+: YAG phosphor-in-glass, Laser & Photonics Reviews, 8 (2014) 158-164. https://doi.org/10.1002/lpor.201300140.

[15] S. Li, Q. Zhu, D. Tang, X. Liu, G. Ouyang, L. Cao, N. Hirosaki, T. Nishimura, Z. Huang, R.-J. Xie, Al 2 O 3–YAG: Ce composite phosphor ceramic: a thermally robust and efficient color converter for solid state laser lighting, Journal of Materials Chemistry C, 4 (2016) 8648-8654. https://doi.org/10.1039/C6TC03215J.

[16] O.B. Shchekin, P.J. Schmidt, F. Jin, N. Lawrence, K.J. Vampola, H. Bechtel, D.R. Chamberlin, R. Mueller-Mach, G.O. Mueller, Excitation dependent quenching of luminescence in LED phosphors, physica status solidi (RRL) – Rapid Research Letters, 10 (2016) 310-314. https://doi.org/10.1002/pssr.201600006.

[17] M. Xu, J. Chang, J. Wang, C. Wu, F. Hu, Al2O3-YAG:Ce composite ceramics for high-brightness lighting, Opt. Express, 27 (2019) 872-885. 10.1364/OE.27.000872.

[18] M.S. Jang, Y.H. Choi, S. Wu, T.G. Lim, J.S. Yoo, Material properties of the Ce^{3+}-doped garnet phosphor for a white LED application, Journal of Information Display, 17 (2016) 117-123. http://doi.org/10.1080/15980316.2016.1205527.

[19] R. Osborne, N. Cherepy, D. Åberg, F. Zhou, Z. Seeley, S. Payne, A. Drobshoff, H. Comanzo, A. Srivastava, Ba (1-x) SrxMg3SiN4: Eu narrowband red phosphor, Optical Materials, 84 (2018) 130-136. https://doi.org/10.1016/j.optmat.2018.06.032.

[20] V. Bachmann, C. Ronda, A. Meijerink, Temperature Quenching of Yellow Ce^{3+} Luminescence in YAG:Ce, Chemistry of Materials, 21 (2009) 2077-2084. https://doi.org/10.1021/cm8030768.

[21] S. Watzke, P. Altieri-Weimar, Degradation of silicone in white LEDs during device operation: A finite element approach to product reliability prediction, 2014 15th International Conference on Thermal, Mechanical and Mulit-Physics Simulation and Experiments in Microelectronics and Microsystems (EuroSimE), (2014) 1-5. https://doi.org/10.1109/EuroSimE.2014.6813779.

[22] W.W. Beers, D. Smith, W.E. Cohen, A.M. Srivastava, Temperature dependence (13–600 K) of Mn4+ lifetime in commercial Mg28Ge7.55O32F15.04 and K2SiF6 phosphors, Optical Materials, 84 (2018) 614-617. https://doi.org/10.1016/j.optmat.2018.07.050.